PASJ: Publ. Astron. Soc. Japan , 1–??,

Observations of Prominence Eruptions with Two Radioheliographs, SSRT and NoRH

Victor V. Grechnev, Arkadii M. Uralov, Vasily G. Zandanov, and Nikolai Y. Baranov
Institute of Solar-Terrestrial Physics, Lermontov St. 126, Irkutsk 664033, Russia
grechnev@iszf.irk.ru
and
Kiyoto Shibasaki
Nobeyama Radio Observatory, Minamimaki, Minamisaku, Nagano 384-1305
shibasaki@nro.nao.ac.jp

(Received 2005 March 30; accepted 2005 November 1)

Abstract

We address simultaneous observations of eruptive prominences with two radioheliographs, SSRT at 5.7 GHz and NoRH at 17 and 34 GHz. Three events are presented: 1997 September 27, 2000 September 4, and 2001 January 14. We analyze them using images observed in microwaves, Hα, images from Extreme ultraviolet Imaging Telescope (EIT) on board Solar and Heliospheric Observatory (SOHO), and white-light images from Large Angle and Spectrometric Coronagraph (SOHO/LASCO). We address three stages of the eruptive process: 1) pre-eruptive ascension; 2) rapid acceleration; 3) free expansion, and the overall kinematics of the ejecta. We estimate the densities and kinetic temperatures of prominences, and also the velocities and accelerations of ejecta. The main body of a prominence is surrounded by low-density cool extensions mixed with the coronal plasma, but the transition from the cool prominence to the hot plasma is sharp. From microwave and LASCO observations with overlapping fields of view we identify a radio prominence and a core of a coronal mass ejection (CME). Their temperature remains at about 5000 K, while the brightenings observed in extreme ultraviolet are probably due to only skin-heating. We discuss the observations in terms of our Dual-Filament CME initiation model.

Key words: Sun: corona — Sun: filaments — Sun: prominences — Sun: coronal mass ejections (CMEs) — Sun: radio radiation

1. Introduction

Comprehensive analyses of filament and prominence eruptions and their relations to coronal mass ejections (CMEs) meet difficulties, because different stages of the eruption are observed with significantly different methods, and the fields of view usually do not overlap with each other. Observations in the Hα line are restricted by the conditions when the optical thickness of a filament/prominence is sufficiently large. For this reason, the motion of eruptive filaments can be rarely observed against the solar disk, mostly in the blue wing of the Hα line, and for rather short distances. The same reason, a decrease of the optical depth, does not permit one to observe the prominence eruptions in Hα at large heights above the limb. White-light observations with currently operating C2 and C3 detectors of the Large Angle and Spectrometric Coronagraph (LASCO) onboard the Solar and Heliospheric Observatory (SOHO) have the opposite limitation of two solar radii. By contrast, microwave radioheliographs can show the whole story of a filament/prominence, including its long life before the eruption and its initial stages, in particular, its detachment from the solar surface. Unlike long-meter wave radio observations (cf., e.g., Marqué et al. 2002; Ramesh 2005), microwaves show processes and structures down to the lower corona and chromosphere. The field of view of a microwave radioheliograph is determined by the geometry of the interferometer and the orientation of the observing direction with respect to its baselines. Under favorable conditions, it can be wide enough to overlap with the field of view of SOHO/LASCO/C2, which promises direct identification of the CME components with features observed in microwaves as well as measurements of their overall kinematics. Although they are long-standing issues, the identification is still not straightforward, and some results published so far (e.g., Gallagher et al. 2003; Kundu et al. 2004; Ma et al. 2005) are difficult to reconcile.

The kinetic temperature of filaments/prominences is generally assumed to be low. Quiescent filaments outside active regions are known to have a temperature of about 5000 K under thermal equilibrium. The temperature of filaments visible in Hα does not exceed 10000 K. In addition, many prominences have been observed by the Extreme ultraviolet Imaging Telescope (EIT) on board SOHO in the 304 Å channel without counterparts in the 195 Å channel (1–2 MK). The 304 Å band includes the HeII line with an excitation temperature of 20000–80000 K and a weaker contribution of the SiXI line (1.6 MK). Hence, the temperature of, at least, some parts of those prominences is between 20000 and 80000 K.

Prominences, filaments, and filament channels are pro-

nounced in microwaves due to their low kinetic temperature and high density as well as the low coronal opacity at frequencies ≥ 5.7 GHz. Thus, they block brighter emission when observed on the solar disk, and produce their own emission well detectable when observed against the sky. They have been well observed with the Nobeyama Radioheliograph (NoRH) and the Siberian Solar Radio Telescope (SSRT), both quiescent and eruptive (Hanaoka et al. 1994; Gopalswamy, Hanaoka 1998; Hanaoka, Shinkawa 1999; Zandanov, Lesovoi 1999; Zandanov et al. 1999; Uralov et al. 2002). The NoRH (Nakajima et al. 1994) and SSRT (Smolkov et al. 1986; Grechnev et al. 2003) are among the World's largest radioheliographs dedicated exclusively to solar observations. They have been operating simultaneously during the solar cycle. The SSRT (5.7 GHz) and NoRH (17 and 34 GHz) observe the Sun with a large observational overlap (the local noon is at $\sim$02:45 UT at NoRH and at $\sim$05:15 UT at SSRT).

Observations of large-scale features with NoRH at 34 GHz are not straightforward, because the fundamental spacing of the interferometer is absent at this frequency. The minimal distance between antennas is too large; hence, the angular distance between adjacent interference order is too small to exceed the solar diameter. Therefore, the solar images produced in adjacent interference orders overlap with each other. For this reason, the background for a prominence at 34 GHz is a superposition of the brightness distributions over the solar disk in the overlapping interference orders, rather than the uniform sky. This circumstance is usually negligible when solar flares are observed, because flaring sources are much brighter than the background features on the disk. For weak features, like prominences, this circumstance becomes important. Therefore, our discussion is related to NoRH observations mainly at 17 GHz; we address three-frequency data for the observations on 1997 September 27 only.

The major (if not the only) emission mechanism of prominences, filaments, and filament channels in microwaves is thermal bremsstrahlung. The optical thickness for thermal free–free emission is determined by a well-know expression, $\tau \propto n_{\rm e}^2 L T^{-3/2} \nu^{-2}$, with ν being the observing frequency, $n_{\rm e}$ the electron density, L the depth of the emitting source, and T its temperature. In the optically thick case, the observed brightness temperature is almost equal to the kinetic temperature, which provides its measurements. Small differences of the brightness temperatures of the prominence body at the SSRT and NoRH observing frequencies are due to the presence of the optically thin coronal plasma. If a feature observed is optically thick at a lower frequency and optically thin at a higher frequency, we also have a possibility to estimate the density of its material. These circumstances determine good opportunities for plasma diagnostics. This is the first advantage of observations with two radioheliographs at distant frequencies, because the optical thickness for free–free emission recorded with the NoRH at 17 GHz and SSRT at 5.7 GHz differs by about one order of magnitude. A significant observational overlap of the SSRT and NoRH provides us with simultaneous observations, which allows realizing the above advantage.

The filaments and prominences are supposed to be optically thick at both 5.7 and 17 GHz (for a typical quiescent filament, $\tau \gg 1$ in microwaves—see, e.g., Rao, Kundu 1977). Their brightness temperatures are usually close indeed. At 5.7 GHz, cool filaments and filament channels show higher contrast and more details, although the spatial resolution of the NoRH at 17 GHz is generally better than that of the SSRT. These facts are obviously explained by the higher contrast with respect to the quiet Sun ($T_{\rm QS} = 16000$ K at 5.7 GHz and $T_{\rm QS} = 10000$ K at 17 GHz) as well as limitations of the CLEAN routine. Filaments with a higher kinetic temperature, about 10000 K, are obviously not visible at 17 GHz, but still visible at 5.7 GHz.

Observations of prominence eruptions at 17 GHz have been discussed in several papers (e.g., Hanaoka et al. 1994; review by Gopalswamy 1999). Some of their results suggest a heating of expanding filaments (Gopalswamy et al. 1998; Hanaoka, Shinkawa 1999). In the present paper, we also address this issue. However, in analyzed cases, the brightness temperatures of the eruptive prominences remained unchanged and close at 5.7 and 17 GHz, which means that their main bodies did not experience heating while they were visible in microwaves (see also Uralov et al. 2002). The brightenings observed for some their parts in EUV could be due to only heating of their skin.

Observations with the two radioheliographs, whose operation principles are very different (synthesis for the NoRH and direct imaging for the SSRT), simplify the detection and elimination of instrumental contributions, when the features of interest appear to be dissimilar in their images. Due to direct imaging, the beam pattern of the SSRT has a relatively low sidelobe level ($\leq 22\%$ with an ideal field distribution). This allows using even "dirty" SSRT images, in which the sources are not very bright. On the other hand, the direct imaging principle results in a very high dynamic range of input signals in the observations of flares. For this reason, it is very difficult to detect filaments when a strong flare occurs, and thus we consider eruptions associated with only no or weak flares, which are known to take place outside of active regions (Švestka 2001).

Up to the present time, about 400 prominence eruptions have been detected automatically[1] in NoRH records. Their detailed analysis by Hori and Culhane (2002) and Gopalswamy et al. (2003) has confirmed a close association between prominence eruptions and CMEs. Several prominence and filament eruptions have also been recorded at the SSRT (at least 20, Kardapolova et al. 2004), but their detection is not automatic so far.

We present and discuss in this paper three simultaneous observations of eruptive filaments and prominences with the two radioheliographs (one of them was discussed previously by Uralov et al. 2002, 2005) and demonstrate their

[1] M. Shimojo, NoRH Observations of Prominence Eruption, ⟨http://solar.nro.nao.ac.jp/meeting/nbym04/index.html⟩.

advantages to shed some additional light on processes of filament eruptions and their relations to CMEs. We also use Hα, extreme ultraviolet (EUV) and white light along with microwave images. We pay attention to the characteristics of the initial stage of the eruption, i.e., the velocity and temperature of an eruptive filament (future core of a CME), initial acceleration, and location of the CME's frontal structure as well as subsequent expansion of the ejecta into the interplanetary space. We use both direct measurements and estimations from appropriate analytical description of observed height-time plots. To discuss the presented events, we briefly mention existing models, compare them with each other, and argue our choice of the Dual-Filament Initiation Model. We briefly outline this model and then discuss the observational findings and results in terms of this model.

2. Observations

2.1. Pre-Eruptive Activation of a Prominence on 1997/09/27

The pre-eruptive activation of a prominence at the western limb on 1997 September 27 was the first event of such a sort observed with the SSRT in the two-dimensional mode. It was also simultaneously observed with the NoRH at two frequencies, 17 and 34 GHz. The sensitivity of the SSRT images that we use was at that time ~ 5000 K, about ten times poorer than that of the NoRH, and the calibration accuracy was also poorer (both significantly improved in 2000). The activation went on during the whole observational daytime of the NoRH and SSRT. The eruption itself occurred when the observations were stopped at both radioheliographs, probably, between 07 and 08 UT associated with a slow CME with the central position angle of 276° and an angular width of 45° registered with LASCO.

2.1.1. EUV, Hα, and microwave images

Some episodes of the prominence activation and eruption are shown in figure 1 using SOHO/EIT in the 304 Å band and Hα images from Mauna Loa and Paris Observatories. As the figure shows, the prominence ascended slowly, and initially had a loop-like shape (the first segment of the prominence). A coarse estimate of the ascension speed for its top between 02:04 and 13:20 UT on September 26 is about 0.3 km s^{-1} in the radial direction. Then, from 13:20 to 19:44 UT, the prominence expanded southwestwards. In the Hα image presented in figure 2, it has a distinct dual-loop (two-segment) shape at 22:26 UT. In the last image where it was visible, Hα of September 27 at 07:44 UT (figure 1f), probably shortly before the eruption, it had a noticeable shape of a horse.

Figure 2 shows the first images of the prominence observed on September 26 with NoRH at 17 GHz (c) and 34 GHz (d) along with an Hα image produced with the Digital Prominence Monitor at the Mauna Loa Solar Observatory (NCAR) (a). Panel (b) shows an overlay of the microwave image at 17 GHz (contour levels at $[2,4,6]\cdot 10^3$ K) on top of the Hα image. The images in microwaves and in Hα are similar, but in microwaves they appear slightly broader, with a great deal of similarity between the 17 and 34 GHz images. However, no manifestations of the spread southwesternmost part visible in 304 Å images (the arrow in figure 1d) are detectable in microwaves and Hα.

As explained in section 1, the NoRH data at 34 GHz have a non-uniform background. In the course of observations, the relative position of the interference orders continuously changes, which results in a motion of the background in the images. Taking this into account, we produced images at 34 GHz with a long integration time of 5 minutes. This allowed us to increase the sensitivity and to partially suppress the influence of the non-uniform background, with an example shown in figure 2d. The solid part of the prominence looks similar at 17 and 34 GHz, but it is not clear whether the sparse environment is a property of the prominence or the non-uniform background.

To estimate the ratio of the brightness temperatures of the prominence at 17 and 34 GHz, we selected sufficiently bright areas ($T_{\rm B} > 1500$ K) to minimize the influence of both the background and gaps (the latter being also due to effects of the CLEAN routine). Then, in our computations, we did not take into account of weaker parts at all. We used the same "mask" at both 17 and 34 GHz. The average brightness temperature computed this way is 2800 K at 34 GHz and 5600 K at 17 GHz. Keeping in mind everything mentioned above, we note that the obtained ratio of 2 can be slightly underestimated, but not overestimated ($T_{\rm B\,17}/T_{\rm B\,34} \geq 2$).

Figure 3 shows the prominence observed at 17 GHz with NoRH in the upper row and at 5.7 GHz with SSRT in the lower row, both with a linear brightness scale. The images shown in figure 3 cover the interval from September 26, 22:31 UT to September 27, 07:19 UT. The first four NoRH images, separated by approximately two hours, were chosen to show the changes in the prominence shape. The last NoRH images were chosen to investigate the correspondence between the NoRH and SSRT observations. During the whole interval, the shape of the prominence gradually transformed, with the most pronounced ascension of the northernmost feature approximately at 50° to the limb. Closer to the end of observations at the SSRT, the prominence took the shape of the horse observed later in Hα (figure 1f). Observations at the NoRH and SSRT did not overlap entirely; hence, no NoRH data are available after 06:22 UT, and no SSRT data are available before 04:53 UT. The first images observed with the SSRT starting from 04:53 UT practically coincide with the image of 05:28:50 UT shown in the figure.

The images appear fragmentary at 17 GHz, while no such fragmentation is visible at 5.7 GHz. However, if a nonlinear representation is applied to 17 GHz images, namely, a power of 0.39, the images observed at the both frequencies become very similar. This suggests that the brightness decreases from the brightest portions of the prominence toward its periphery at 17 GHz steeper than at 5.7 GHz. This is also confirmed by figure 4, where scans at both frequencies are shown crossing a part of the prominence in the band shown in figure 4a with dash-dotted

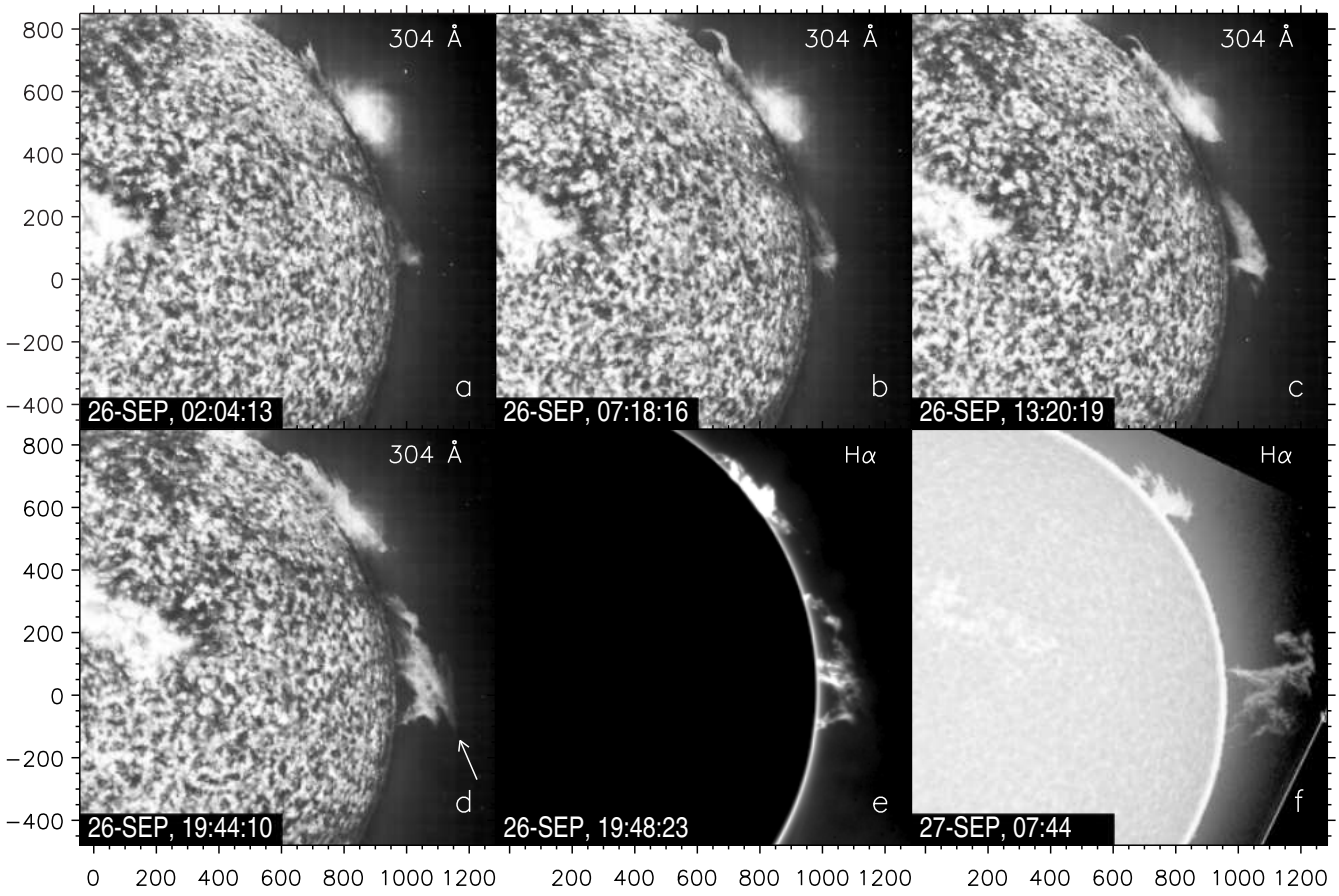

Fig. 1. Snapshots of the 1997 September 27 prominence eruption from SOHO/EIT at 304 Å(a–d) and Hα images (e–Mauna Loa; f–Paris Observatory). The arrow (d) points out the expanding southwesternmost feature. The axes show arcsec from the solar disk center.

lines. To suppress the noise in the SSRT scan, we averaged 5 images from 05:28:50 to 05:50:48 UT and smoothed the scan over 5 points. The SSRT scan at 5.7 GHz is significantly wider than that of the NoRH at 17 GHz, although the difference of the beam widths is small at that time.

2.1.2. Measurements of flux and height

Figure 5 shows some plots that characterize the evolution of the prominence measured at 17 and 5.7 GHz. For the reasons mentioned above, we did not estimate these quantities for the whole day at 34 GHz, (otherwise, each point of the plots should be carefully checked). The upper panel (a) shows the ascension of the prominence. The measurements are related to the northernmost bright feature and to the direction of 50° with respect to the limb. The height was measured from fixed-base difference images (the first frame subtracted) using the "center-of-gravity" technique. The height-time plot shows that the speed was initially about $0.7\,\mathrm{km\,s^{-1}}$, and then, after about 01 UT, it increased to $\sim 3.9\,\mathrm{km\,s^{-1}}$.

The total flux was measured in a straightforward way. The ratio of the total fluxes at 5.7 and 17 GHz is about 1.7. In computations of the average brightness temperatures, sufficiently bright parts of the prominence were only processed, i.e., those with $T_\mathrm{B} \geq 2500$ K at 17 GHz and those with $T_\mathrm{B} \geq 5000$ K at 5.7 GHz. The average brightness temperatures were about 5000 at 17 GHz and about 7000 at 5.7 GHz. Both the total flux and brightness temperature slightly increased before 02 UT, and then slowly declined up to the end of the observations.

2.2. Filament eruption on 2000 September 4

This event, previously discussed by Uralov et al. (2002, 2005), is a filament eruption observed on the solar disk. Some images and plots for this event were also presented by Grechnev et al. (2003). The filament that served as a source for the CME core was quiescent starting from its appearance on the solar disk on 2000 August 26. On September 4, the filament was located in the western area of a giant filament channel extending behind the northeastern limb. No active region was observed there. The event started with activation and a slow rise of the filament. The NoRH and SSRT recorded the motion of the filament across the solar disk and its subsequent expansion against the background of the sky.

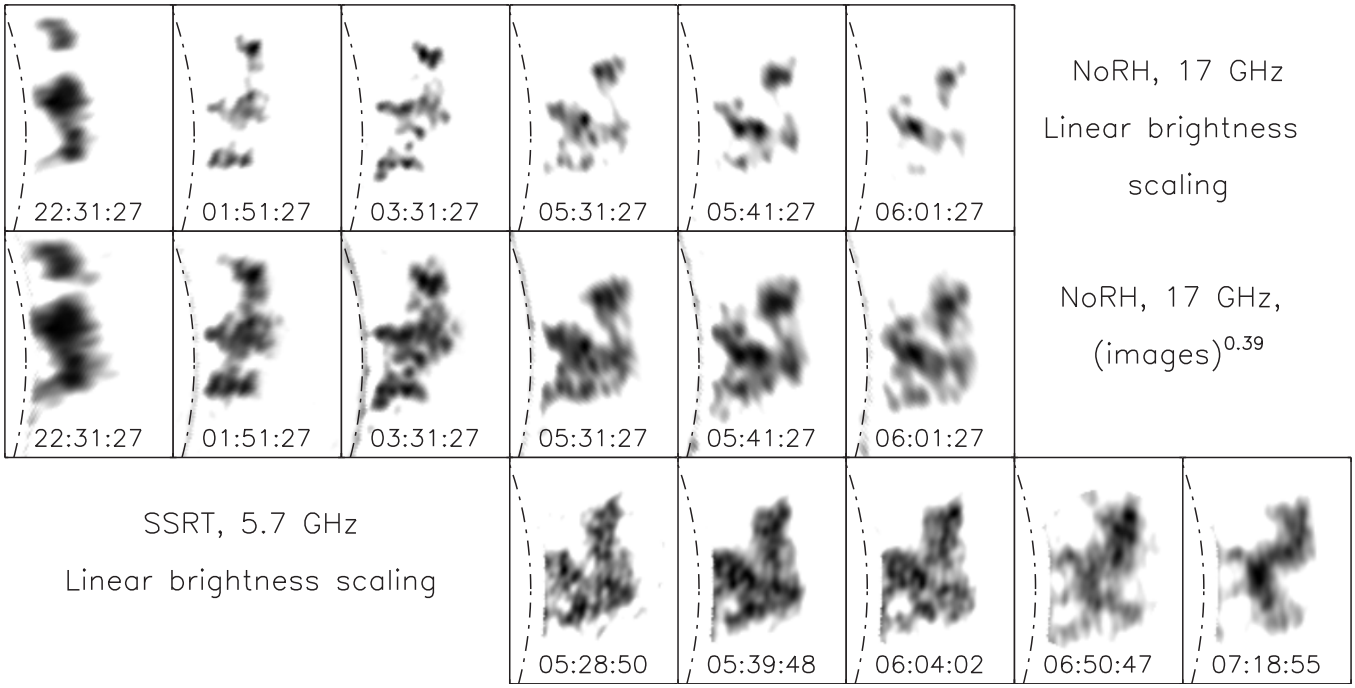

Fig. 3. Negative images of the prominence observed with NoRH at 17 GHz (upper row) and with SSRT at 5.7 GHz ("dirty" images, lower row) in the linear brightness scale. The middle row shows the same 17 GHz images as in the upper row, but in a power-law representation (power of 0.39), which look similar to those of 5.7 GHz shown in the lower row. Images in the columns correspond to close times. The solar disk is removed. The dash-dotted line shows the solar limb.

2.2.1. Microwave and EUV images

Figure 6 illustrates the microwave observations of the event at 5.7 GHz (SSRT, upper row) and 17 GHz (NoRH, middle row) as well as EUV observations with SOHO/EIT at 195 Å (lower row). The range of the observed brightness temperatures in microwaves is wide, and at 5.7 GHz it is more than one order of magnitude wider than that at 17 GHz. Therefore, to show better the low-contrast eruptive filament, we limited the brightness temperatures for both the SSRT and NoRH images, which resulted in a blurring of artificially saturated radio sources. The images clearly show the movement of the eruptive filament and the development of a post-eruptive flare (although the fields of view in the first SSRT frame and last NoRH frames are not sufficient to show the filament fully). The images of the eruptive filament at 5.7 and 17 GHz against the solar disk are similar, likely due to the opacity of the body of the filament at both frequencies. However, the eruptive filament at 5.7 GHz appears broader than at 17 GHz again.

The eruptive filament is also well visible in the first three SOHO/EIT 195 Å fixed-base difference images with the base image of 04:59:35 UT being subtracted (figure 6, lower panel). To suppress the influence of the displacement of bright features due to the solar rotation and to show the filament better, we compensated the solar rotation in images to 06:00 UT and limited the brightness range in the images [the technique described by Chertok and Grechnev (2005)]. There are faint bright features in EIT images associated with the moving ejecta (labeled in figure "BF"). The arc-like feature "BF1" in the EIT frame at 05:23:34 UT was displaced and expanded in the next frame ("BF2"). It ran well ahead of the filament. Uralov et al. (2005) argue that this feature represents the frontal structure of the CME. Also note that the faint bright features visible in the next two frames and obviously associated with the filament. The feature "BF3" has a bent shape (its northern part is difficult to detect) and coincides in the shape and location with the filament observed at 17 GHz. The bright feature "BF4" in the EIT frame of 05:59:21 UT is also cospatial with the filament visible at 5.7 GHz (the field of view of the NoRH in this frame is insufficient to catch this feature).

2.2.2. SSRT and LASCO images

Figure 7 shows LASCO/C2 and SSRT images of the eruption. Actually, there were two segments of the initial eruptive filament, which formed a dual-loop-like structure. The greatest part of the eruptive prominence was concentrated in the western segment, which is better seen in microwaves both on the solar disk and above the limb. This segment of the eruptive prominence is also better visible in SOHO/EIT 195 Å images. The movement of the fainter eastern segment outside of the solar limb is traceable in microwaves when viewing a 5.7 GHz movie, but it is difficult to trace these segments separately on the solar disk, where their envelope is seen as the initial eruptive filament (figure 6).

The eruptive prominence appeared as an expanding dual-filament structure in LASCO/C2 images as well.

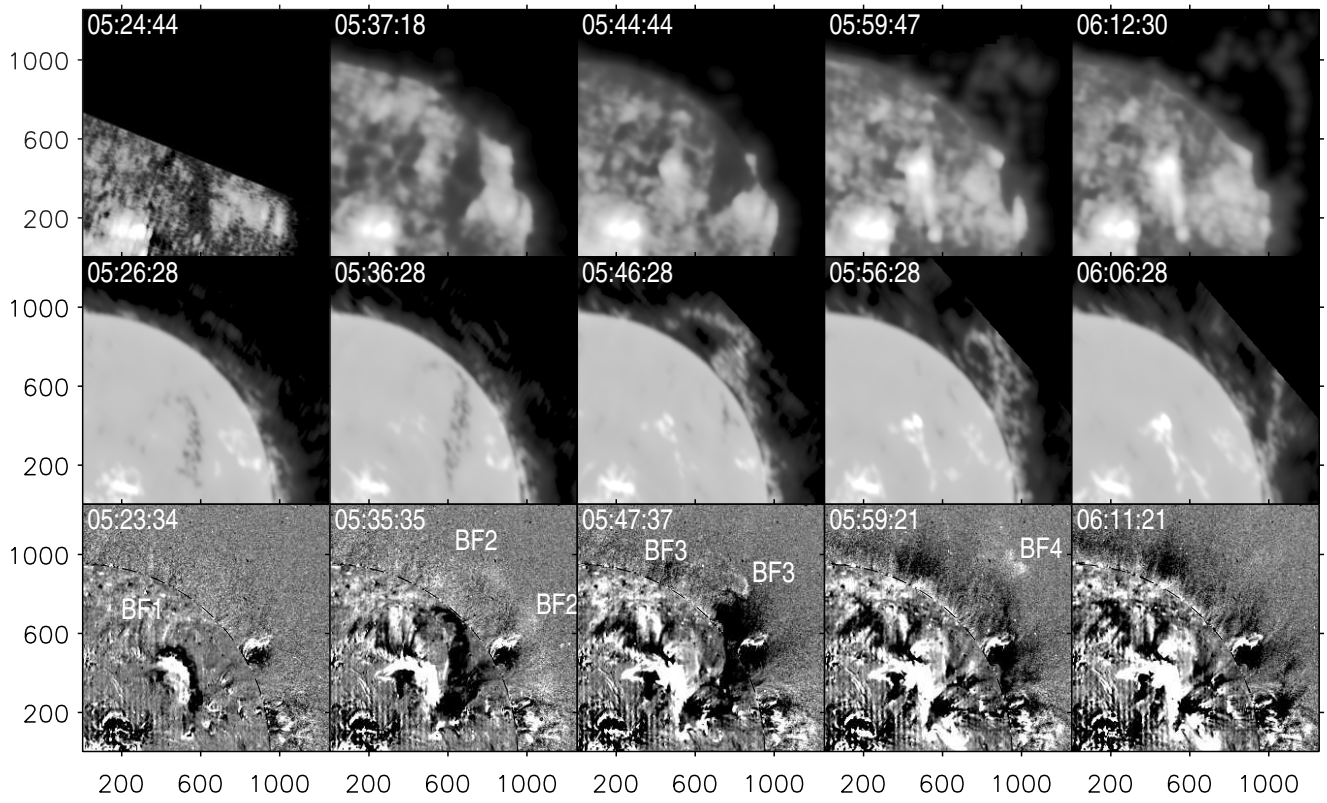

Fig. 6. Some episodes during the evolution of a prominence that erupted on 2000/09/04 observed in microwaves at 5.7 GHz (upper row, first "dirty", others "clean" images) and 17 GHz (middle row). The lower row shows fixed-base (04:59:35 UT) SOHO/EIT 195 Å difference images derotated to 06:00 UT. Bright features visible in the SOHO/EIT are labeled "BF". Black dashed lines in the lower row denote the solar limb. The axes show the distance from the solar disk center in arcsec.

This structure consisted of two contacting segments sequentially disposed along the edge of the occulting disk (figure 7). The filaments were distinctly connected to each other. The frontal structure of the CME ("S") at its early appearance in LASCO/C2 images has a great deal of similarity with the dual-segment shape of the eruptive filament. Prior to the eruption, the filament did not show any helical structure in either microwaves or EUV. During the eruption, the helix-like shape formed can be revealed in EIT images (Uralov et al. 2002). The shape of the filament became similar to a rope with sharp edges.

2.2.3. Measurements of flux and height

The eruption was followed by a weak (C1.5 in soft X-rays) large-scale two-ribbon flare associated with the formation of a post-eruptive arcade (saturated in EIT images due to the limited brightness range). The flare evolved at the initial location of the eruptive filament, with no active region in the vicinity (see figure 6). It started in microwaves as two compact bright kernels at about 05:25 UT near the bend of the initial filament. After 05:40 UT, the flare ribbons expanded out of these kernels. The absence of strong magnetic fields (as compared with those in active regions) determined, in fact, entirely the thermal character of its microwave emission (cf. Švestka 2001). This is also confirmed by the closeness of the microwave flux to the thermal radio flux predicted by GOES soft X-ray data (figure 8a). The total radio flux was computed as

$$S_{[\mathrm{sfu}]} \approx 7.22 \times 10^{-11} \nu^2_{[\mathrm{GHz}]}\, \rho^2_{[\mathrm{arcsec}]} \sum_i T_{\mathrm{B}i[\mathrm{K}]}, \qquad (1)$$

where $T_{\mathrm{B}i}$ is the brightness temperature of a pixel (with a width ρ), and the thermal radio flux was computed from soft X-ray data as

$$S_{[\mathrm{sfu}]} \approx 3 \times 10^{-45} EM_{[\mathrm{cm}^{-3}]} T^{-1/2}_{[\mathrm{K}]}. \qquad (2)$$

The temperature T and emission measure EM of the emitting plasma were computed from GOES data using the GOES software by R. Schwartz. The light curves computed from SSRT and GOES data are smoothed over five points to suppress jumps due to insufficient accuracy of the calibration and computations. The level of the quiet Sun was subtracted from both SSRT and NoRH data. The presence of the dark filament in the region of the event before the flare determines the negative values of the pre-flare total flux.

Figures 8b–d show height-time plots of the eruptive filament and the frontal structure of the CME. Panel (b) shows the height-time plots measured manually. The positions of the filament are marked with circles (SSRT) and triangles (LASCO), and those of the frontal structure are marked with squares (EIT, bright features "BF1" and

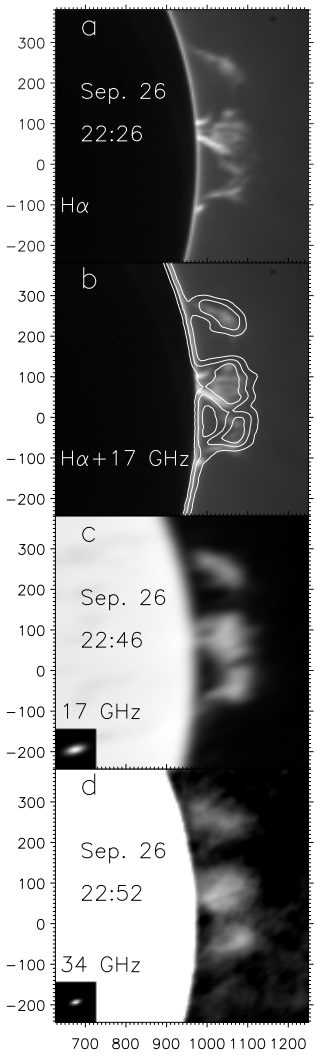

Fig. 2. Prominence observed late on September 26 in Hα (a) and at 17 and 34 GHz (NoRH, c and d). Panel (b) shows an overlay of the Hα and 17 GHz images of (a) and (c), with contour levels at 2000, 4000, 6000 K. The small insets in the lower-left corners of the microwave images show the NoRH beam.

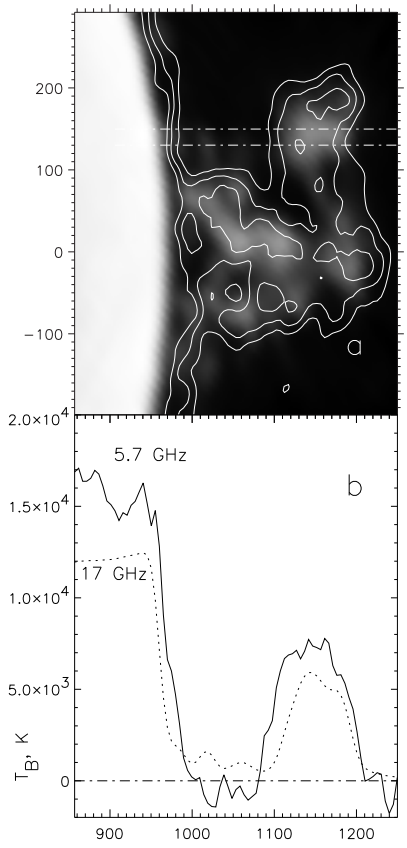

Fig. 4. Cross sections (b) of the prominence observed at 17 GHz (a, gray scale, 05:41 UT) and 5.7 GHz (a, contours of 3000, 5000, 7000 K, 05:47 UT). The scans were computed in the band marked with dash-dotted lines in panel (a).

"BF2" in images of 05:23:34 and 05:35:35 UT in figure 6) and crosses (LASCO). The horizontal axis shows the universal time, and the vertical axis shows the distance from the solar disk center. Panel (c) shows the comparison of the measured height-time plots with self-similar invariant kinematic plots (see Uralov et al. 2005). The vertical axis shows the dimensionless coordinate $x = R/R_0$ with R being the distance measured from the virtual expansion center, which is located below the solar surface at a depth of about 50 Mm. The $R_0 \approx 150$ Mm is the initial radius of the CME's frontal structure. The horizontal axis shows the dimensionless time, $(t-t_0)/\tau$, with $\tau = R_0/U_\infty \approx 170$ s being the initial time scale of the CME, $t_0 \approx 05{:}19$ UT being the onset time of the self-similar expansion, and U_∞ being the asymptotic velocity of the CME. Panel (d) shows the initial part of the preceding plot. Note that the self-similar solution has no meaning at $t < t_0$. Hence, the X axes in figures 8b–d have, in principle, no extensions leftwards. Nevertheless, we have plotted the points observed earlier than t_0 to show the motion of the prominence before onset of the self-similar expansion, and to show the quality of the fit. From a comparison of the total flux time profile shown in figure 8a with the height-time plot in figure 8b we see that the microwave flux started to increase approximately at the same time as the filament acquired rapid acceleration (vertical dashed line in figure 8b) within the accuracy of measurements (a few minutes).

2.3. Event of 2001 January 14

The 2001 January 14 prominence eruption occurred not far from the north pole. The prominence was not associated with any active region. After the eruption, a long post-eruptive arcade was observed in soft X-rays and extreme ultraviolet, but the soft X-ray flux was weak, C1.4 (cf. Švestka 2001), and no Hα flaring was registered. The event was observed with SSRT, NoRH, SOHO/EIT & LASCO, Yohkoh/SXT, and at Yunnan Observatory in Hα.

Quite recently, Ma et al. (2005) briefly addressed this eruption using SOHO/EIT & LASCO, Hα, and 17 GHz NoRH data. The authors measured the kinematic charac-

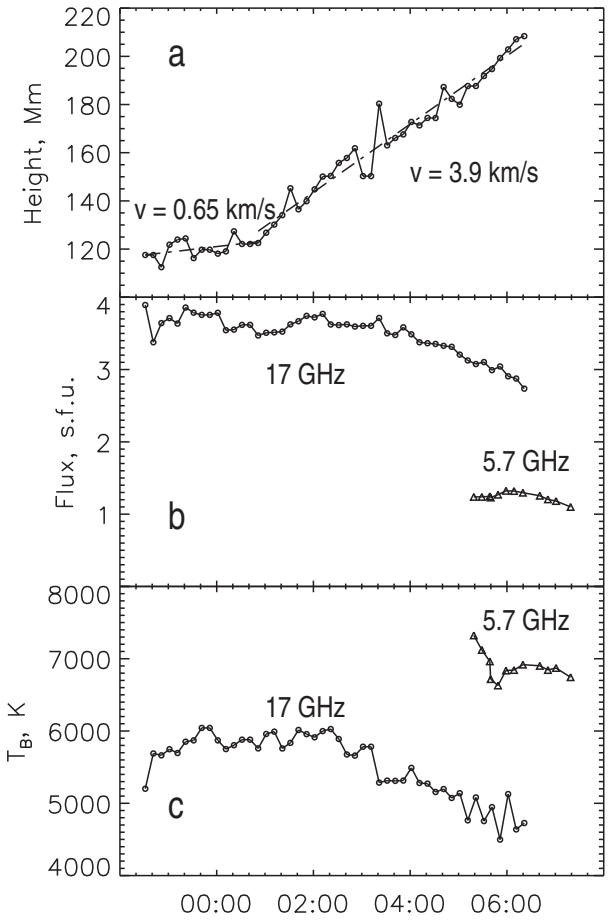

Fig. 5. Parameters of the active prominence observed on September 27, 1997 at 17 and 5.7 GHz. (a) Ascension of the prominence measured from the NoRH images at 17 GHz, (b) its total flux at 17 and 5.7 GHz, (c) the average brightness temperatures at 17 and 5.7 GHz.

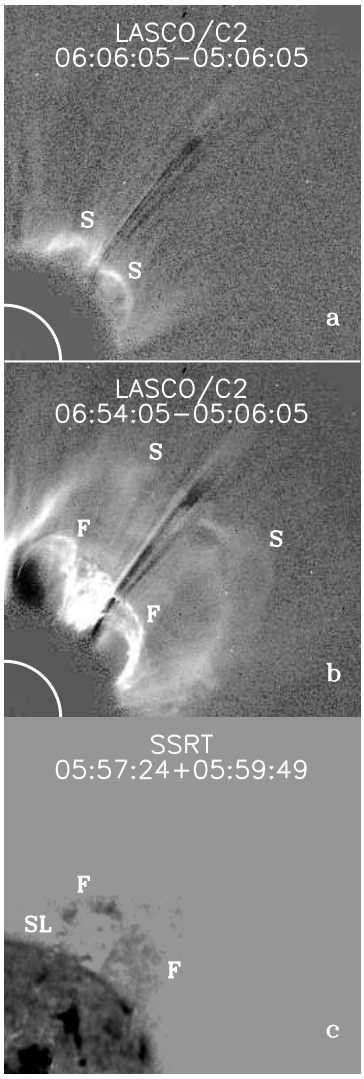

Fig. 7. LASCO/C2 and SSRT ("dirty", negative) images of the eruption observed on 2000 September 4. A fixed-base difference SOHO/LASCO/C2 white-light image shows the appearance of the frontal structure "S" above the occulting disk of LASCO (a), next the eruptive filament "F" (b). The NW quadrant is only shown. Note that an extended feature "SL" is a sidelobe of the SSRT beam.

teristics of the prominence from EIT 195 Å images. They found the speed to increase from zero (before 04:30 UT) to 180 km s^{-1} at 06:30 UT. The acceleration plot of the prominence measured by Ma et al. (2005) consists of two linear parts, one increasing from zero to about 10 m s^{-2} between 04:30 UT and 05:25 UT, and another one increasing to 70 m s^{-2} at 06:30 UT. From the apparent closeness of the legs of the CME core (LASCO/C2) and prominence (EIT 304 Å) they concluded that the CME core was the erupting cool, dense prominence material in the outer corona. They also pointed out that this was a fast CME, although it correlated with the prominence eruption without a flare. However, the authors confused two different CMEs, the CME's frontal structure with the prominence, and missed the fact that some parts of the eruptive prominence were bright in EIT 195 Å images, which suggests their kinetic temperature of order 1 MK. The latter circumstance appears to be contradictory to the conclusion of Ma et al. (2005) about cool CME core, which does not seem to be well-grounded. For these reasons, this eruption should be carefully analyzed. A remarkable feature of this event is that the fields of view of the SSRT and

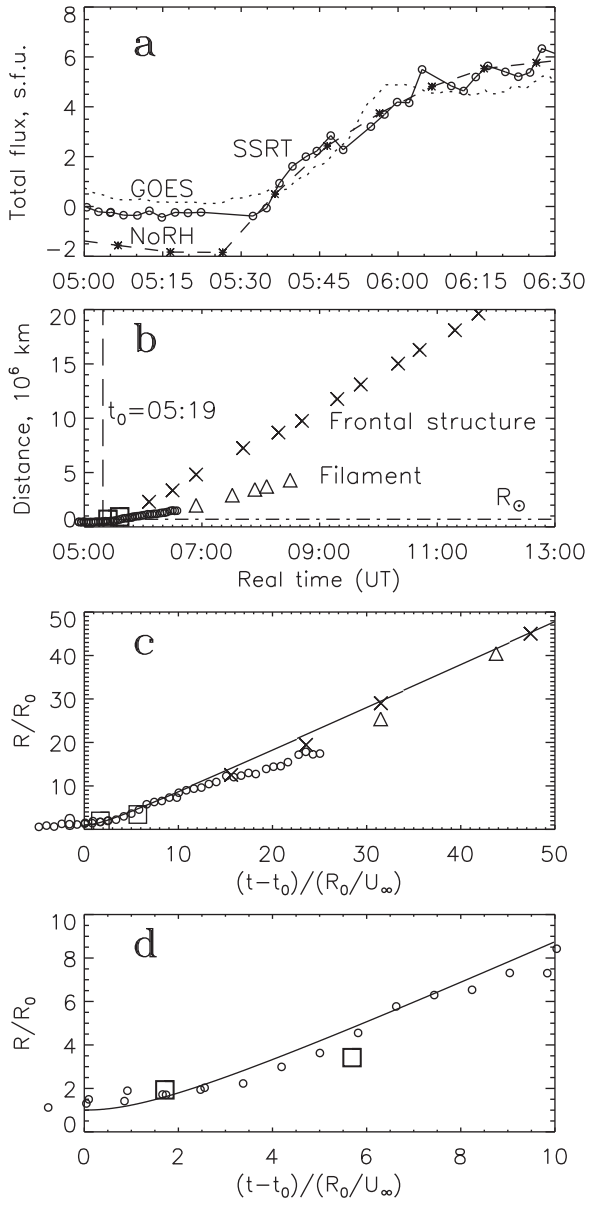

Fig. 8. (a) Event of 2000 September 4. (a) Total flux of the post-eruptive flare at 5.7 (solid) and 17 GHz (dashed) and the thermal radio flux predicted by GOES data (dotted). (b) Observed height-time plots. Filament: circles (SSRT) and triangles (LASCO), frontal structure: squares (EIT) and crosses (LASCO). The vertical axis shows the distance from the solar disk center. c) Comparison of the observed height-time plots with self-similar invariant kinematic plots. The axes show the dimensionless time and coordinate. (d) Same as (c), the initial part.

LASCO/C2 overlapped, so the eruptive prominence was observed simultaneously with both of these instruments.

2.3.1. Related CMEs

We conclude that there were at least three successive CMEs in the northwestern sector at close times. First, a very slow, faint CME with a central position angle of $\simeq 310°$ and an angular width of about 30° appeared at 03:54 UT. Then, a brighter CME occurred, which was associated with the eruption of our interest. It had a central position angle of $\simeq 330°$ and an angular width of about 90° (the first appearance in LASCO/C2 images at 06:30 UT). Finally, at 06:54 UT, much faster CME appeared in LASCO/C2 images with a central position angle of 355°. The speed of its frontal structure increased from 700 to 1200 km s^{-1} during LASCO observations. Probably, due to this triple character, the first and second CMEs are not registered in LASCO catalogs. The second and third CMEs were probably associated with the same extended region near to the north pole, but the second CME ejected from its western part, while the third one ejected from its eastern part. Considering the second statement of Ma et al. (2005), note that the third, fast CME with a central position angle of 355° should be classified, following Švestka (2001), as triggered by a propagating disturbance (e.g., wave-like) from the prominence eruption of interest, rather than by this eruption itself. Complex disturbances over a huge area in the northern hemisphere are visible in EIT 195 Å movie available at the SOHO Web site.

2.3.2. Microwave and EUV images

Figure 9 shows the event in the same format as figure 6. The upper row shows 5.7 GHz images, the middle row shows 17 GHz images, and the lower row shows EIT 195 Å fixed-base difference images. The average brightness temperature at 17 GHz is 4700 ± 200 K. The average brightness temperature at 5.7 GHz is about 5300 K until 06:50 UT. The figure shows qualitatively that the brightness temperatures of the prominence observed at the both frequencies remain constant in all the frames shown. Only after 06:50 UT, the brightness temperature at 5.7 GHz started to decrease, likely due to a decrease in the opacity of the prominence during the course of its expansion and disintegration.

Figure 10 shows more frames of the eruptive prominence observed at 5.7 GHz in a wider field of view. The eruption was recorded with SSRT in about fifty frames, and 16 of them (all "dirty" images) are shown in the figure. We show the brightness temperature range from 0 to 15000 K. Fragments of the prominence in the figure can be detected up to two solar radii from the solar disk center.

2.3.3. SSRT and LASCO images

Figure 11 shows in panel (a) the combination of an SSRT image observed at 06:53 UT with a LASCO/C2 image of 06:54 UT. In panel (b), the SSRT image of 07:26 UT and the closest LASCO/C2 image of 07:31 UT are shown. One can see that the fragment of the eruptive prominence

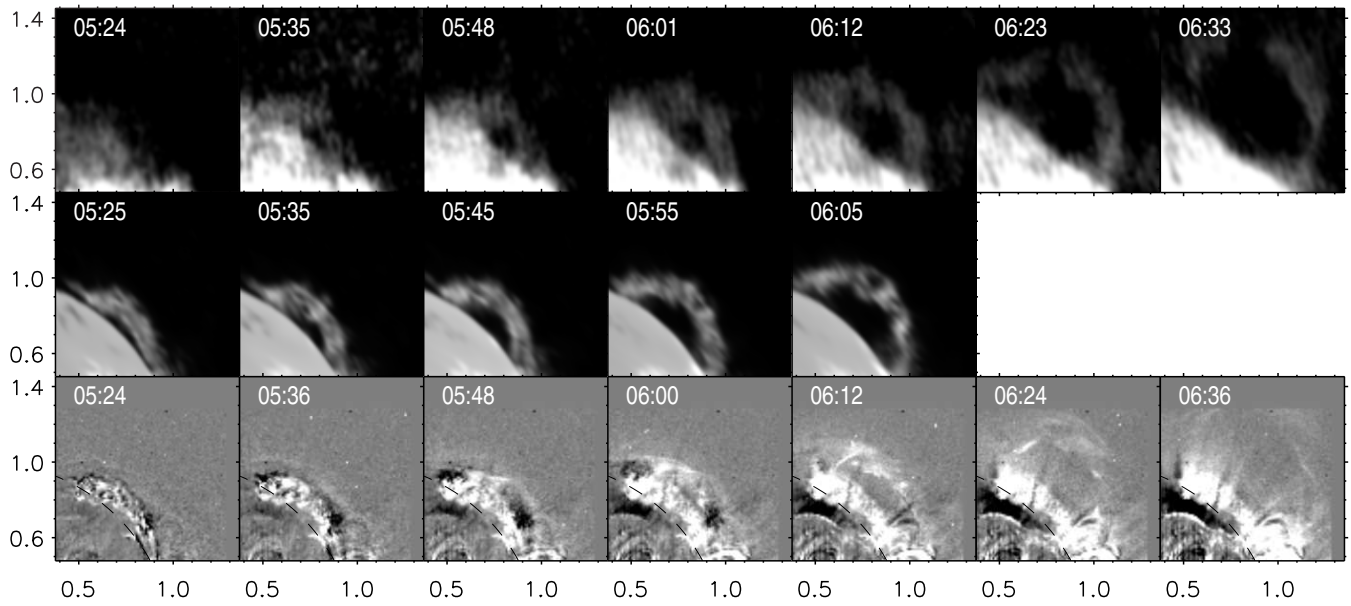

Fig. 9. Images of a prominence that erupted on 2001/01/14 observed in microwaves at 5.7 GHz (upper row, "dirty" images) and 17 GHz (middle row). The lower row shows fixed-base (04:36 UT) SOHO/EIT 195 Å difference images derotated to 06:10 UT. The black dashed lines in the lower row denote the solar limb. The axes show the distance from the solar disk center in solar radii.

visible at 5.7 GHz passes into the CME core visible in white light with LASCO, and coincides with it where their fields of view overlap. To make sure, one can compare the shape of the filament in the SSRT images with its evolution in figure 10. The figure also shows qualitatively the constancy of the brightness temperature of the prominence. This confirms again that the CME core is the eruptive prominence (filament) or its observed remnants (e.g., Gopalswamy et al. 1998; Gopalswamy et al. 2003).

2.3.4. Measurements of flux and height

Figure 12 shows some plots for the eruptive prominence measured from 17 GHz, 5.7 GHz, and LASCO images. Figures 12a,b show the height-time plots for the distance of the fastest feature of the eruptive prominence from the solar disk center measured from the SSRT (circles) and LASCO/C2 (squares) images. Note that it is difficult to measure the initial part of the prominence motion, because the velocity is small. It is also difficult to accurately measure the height-time plot for the CME core from LASCO images, due to its disintegration as well as contamination (and, probably, interaction) with the first and third CMEs. For this reason, we measured all of the heights manually. The frontal structure is rather easily detectable in difference LASCO images (we used both fixed-base and running differences). As for the core, we adjusted the brightness range in each image to detect its threadlike structure, and measured its height.

We estimate the initial acceleration for the prominence measured from NoRH images of about $10\,\mathrm{m\,s^{-2}}$ at 04:15. It then increased in the latest NoRH images up to about $40\,\mathrm{m\,s^{-2}}$ at 06:00. The acceleration measured from the SSRT data is nearly constant for more than one hour, about $60\,\mathrm{m\,s^{-2}}$. The second order fit for this part is shown in figure 12a with a dotted line. The maximum speed of the prominence in SSRT images is $280\,\mathrm{km\,s^{-1}}$. The acceleration estimated for the core of the second CME from LASCO images is $< 1\,\mathrm{m\,s^{-2}}$, and the final speed is $\sim 550\,\mathrm{km\,s^{-1}}$. The final speed of the frontal structure is $\sim 790\,\mathrm{km\,s^{-1}}$. The kinematic characteristics we measured are in the overall agreement with the results obtained by Ma et al. (2005) for the prominence from SOHO/EIT 195 Å data, but, of course, different for the frontal structure. Small differences related to the prominence could be due to the fact that Ma et al. (2005) measured them from EIT 195 Å images, where bright, hot parts of the EUV prominence may differ from the cool radio prominence.

Figure 12c shows the time profile for the total flux of the eruptive prominence measured from the NoRH 17 GHz images. The plot does not contain the contribution of the solar disk. The increase in the total flux by a factor of 1.8 along with the constancy of the average brightness temperature means the corresponding increase in the area of the eruptive prominence.

3. Discussion

3.1. Temperature and Density

Two- and three-frequency microwave data allowed us to estimate the kinetic temperature of the erupting filament. For all three eruptive prominences, no heating was observed of their main body. On the other hand, SOHO/EIT shows some brightenings of the eruptive prominences for both the 2000 September 04 and 2001 January 14 events, which are cospatial with their parts observed with close brightness temperatures of 5000–7000 K at 5.7 and 17 GHz. The latter circumstance means that the bulk of their body is cool, and a natural explanation

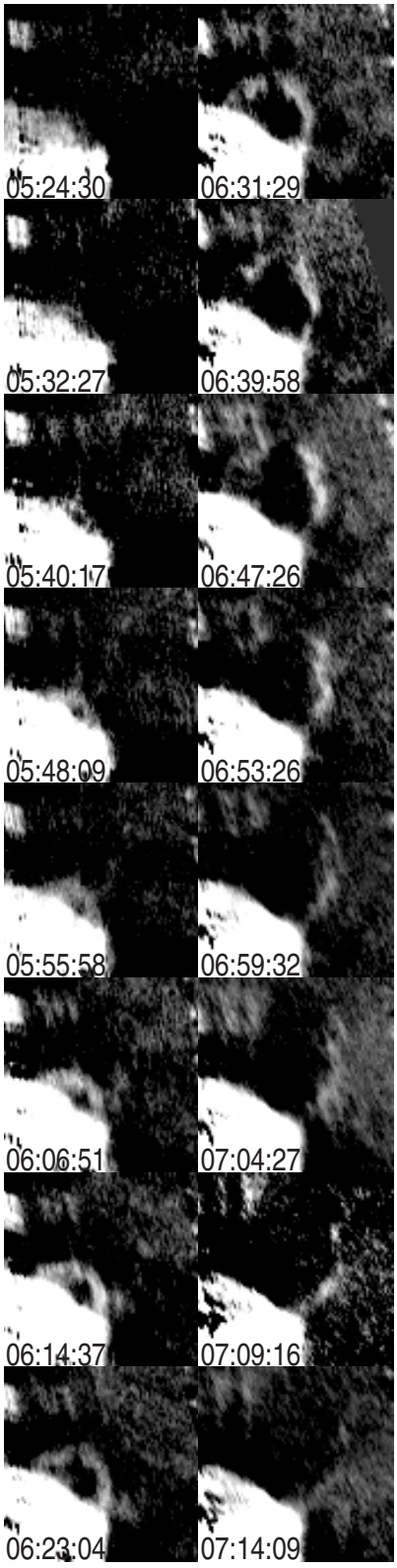

Fig. 10. Observations of the eruptive prominence on 2001 January 14 with SSRT (16 of 54 frames, each third frame, all "dirty"). The field of view is $845'' \times 845''$.

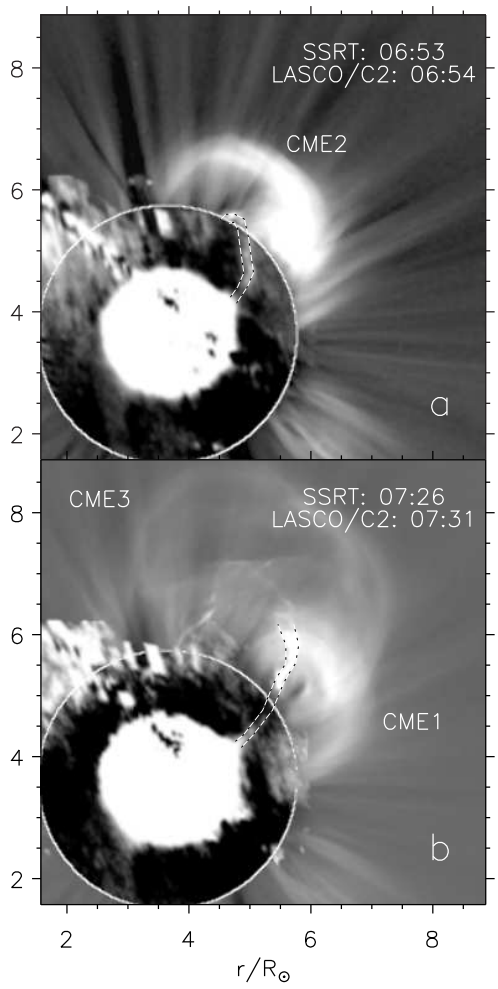

Fig. 11. Superposition of SSRT and LASCO/C2 images of the eruption observed on 2001 January 14. The dotted lines trace the eruptive prominence in SSRT images and the core of the CME in LASCO/C2 images. Two closest frames are shown (a and b). The axes show the distance from the solar disk center in fractions of solar radii.

of these EUV brightenings of the eruptive prominences is heating of only their thin envelopes, whose contribution is negligible in microwaves. This conclusion is supported by the fact that the brightened eruptive filaments and prominences observed sometimes in EUV (e.g., well-known TRACE movies of 2001/04/15, 22:05–22:20 UT; 2002/08/16, 10:20–11:50 UT) do not become transparent, which one could expect if they are heated entirely. Instead, the observations suggest the presence of cool material behind the bright envelope, which is opaque for farther emitting structures due to absorption by hydrogen and helium continua in the cool plasma of the filament (see also Mein et al. 2004).

3.1.1. Event of 1997/09/27

A comparison of 17 GHz and 5.7 GHz images of this active prominence has revealed the following.

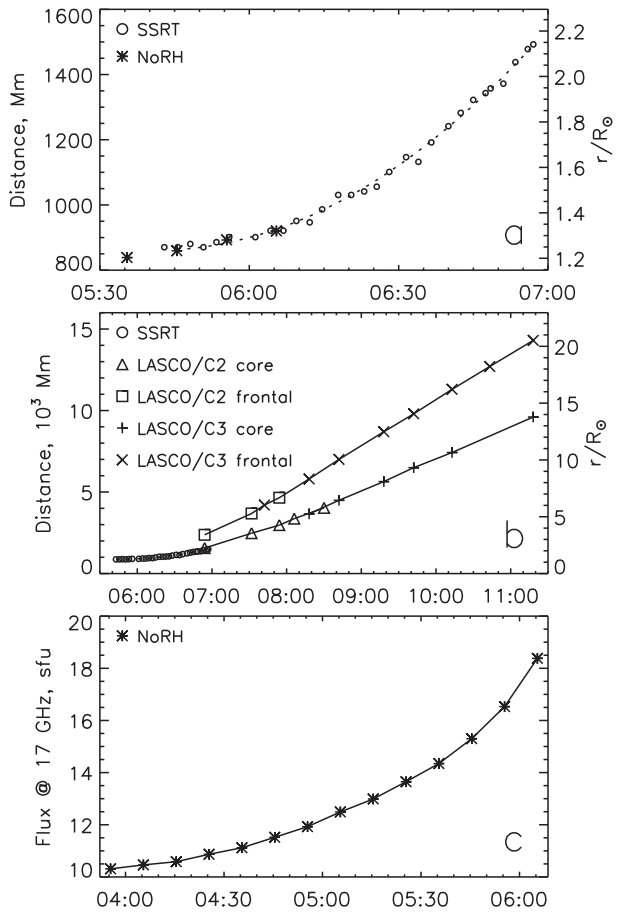

Fig. 12. Event of 2001 January 14. (a,b) Height-time plots measured from the SSRT, NoRH, and LASCO/C2 & C3 data. (c) The 17 GHz total flux time profile for the eruptive prominence.

1. The prominence is wider at 5.7 GHz with (a) its main body being optically thick at both frequencies and roughly coinciding with the Hα prominence, and (b) some of its surrounding detected at 5.7 GHz and confirmed by 17 GHz images.
2. The difference of the brightness temperatures, $\Delta = T_{\rm B\,5.7} - T_{\rm B\,17} \approx 2000$ K, for the main body of the prominence.

Note that filaments on the solar disk have similar properties (see, e.g., Chiuderi-Drago, 1989; Gary 1986; Zandanov et al. 1999), i.e., their brightness temperatures and sizes decrease with the frequency.

From a comparison of the 17 and 34 GHz images we have found $T_{\rm B\,17}/T_{\rm B\,34} \approx 2$ for the main body of the prominence. This ratio is between ≈ 1 and 4, with ≈ 1 being for the optically thick limit at both frequencies, and 4 for the optically thin limit. This means that the prominence opacity decreases within the range of 17–34 GHz, and it is optically thin at frequencies > 34 GHz. Hence, we can roughly estimate the column emission measure for the main body of the cool prominence, taking its optical depth as $\tau \approx 1$ at 34 GHz, $EM \approx 1.5 \cdot 10^{28}$ cm^{-5}. There is a large uncertainty in its geometrical depth, which we cannot infer from our observations. Taking the probable limits of $1.5 \cdot 10^8$ cm to $1.5 \cdot 10^9$ cm, known from observations of filaments on the solar disk, we obtain the electron density of $n_{\rm P} = (1\text{–}3) \cdot 10^{10}$ cm^{-3}.

Again using the similarity of prominences observed against the sky and filaments observed on the solar disk, we can estimate the characteristics of the prominence-to-corona transition region (PCTR) from the dense plasma of the cool prominence to sparse plasmas of the hot corona surrounding the prominence. It seems that the difference in the sizes for the prominence observed at 17 and 5.7 GHz is due to an extended transition between the prominence and the corona, but this is not true, as the following estimation shows.

The small difference of the brightness temperatures observed at 17 and 5.7 GHz of $\Delta \approx 2 \cdot 10^3$ K inside the optically thick main body of the prominence is a sum of two components, the PCTR contribution of $\delta_{\rm PCTR}$, and the coronal contribution of $\delta_{\rm c}$: $\Delta = \delta_{\rm PCTR} + \delta_{\rm c}$ (both optically thin in our case). Assuming a constant gas pressure and linear growth of the plasma density inside the PCTR, we find $\delta_{\rm PCTR} \approx (2/7)\alpha\xi\mu_{\rm P} L T_{\rm P}$ with

$$\alpha = 1 - \frac{\lambda_{17}^2}{\lambda_{5.7}^2} \approx 0.9,\ \xi \approx 1 + \frac{n_{\rm c}}{n_{\rm P}} \approx 1,\ \mu_{\rm P} \approx 3 \cdot 10^{-22} \frac{n_{\rm P}^2 \lambda_{5.7}^2}{T_{\rm P}^{3/2}} \,{\rm cm}^{-1} \quad (3)$$

Here, $T_{\rm P}$ and $n_{\rm P}$ are the kinetic temperature and the electron number density in the prominence, $\mu_{\rm P}$ is the free–free absorption coefficient in the prominence, and $n_{\rm c}$ is the plasma number density at the outer boundary of the PCTR, whose depth is L.

The contribution of the isothermal corona with a temperature of $T_{\rm c}$ and density exponentially decreasing along the line of sight, $n_{\rm c} \exp(-x/\Lambda)$, is equal to

$$\delta_{\rm c} \approx \frac{1}{2} \alpha \mu_{\rm c} \Lambda T_{\rm c}, \quad \mu_{\rm c} = \mu_{\rm P} \frac{n_{\rm c}^2}{n_{\rm P}^2} \quad (4)$$

with $\mu_{\rm c}$ being the free–free absorption coefficient at the boundary of the corona and PCTR.

Taking for the estimations $n_{\rm P} = (1\text{–}3) \cdot 10^{10}$ cm^{-3}, $n_{\rm c} = 10^8$ cm^{-3}, $T_{\rm P} = 5600$ K which is close to $T_{\rm B\,17}$ inside the main body of the prominence, $T_{\rm c} = 10^6$ K, $\Lambda = 10^{10}$ cm, we obtain $\delta_{\rm c} \approx 700$ K; hence, $\delta_{\rm PCTR} \approx 1300$ K. The depth of the PCTR of $L \leq 5$ km corresponds to the obtained $\delta_{\rm PCTR}$; thus, the transition from cool to much hotter plasmas must be very sharp. Note that this is related to the thickness of the major layer of the prominence-to-corona transition region, which contributes to microwaves.

One could suppose that L is small in the direction perpendicular to the plane of the prominence, but comparable with the vertical extent of the radio prominence observed at 5.7 GHz. However, if it would be so, then the brightness temperatures of the filament observed on the solar disk must be unrealistically high, which is not the case.

The reason for the difference in sizes observed for the prominence at 17 and 5.7 GHz can be an extension of the prominence both upward and downward, which is optically thin at 17 GHz, but contributes appreciably at 5.7 GHz. On the other hand, it is not clear which compo-

nent of the solar plasma is the source of this emission. We guess that it can be the cold material of the same prominence that is scattered in numerous threads surrounding its main body both from below (filament barbs) and above with an electron density of order $(2–8)\cdot10^9\,\mathrm{cm}^{-3}$. The spectroscopic observations reported by Kurochka and Kiryukhina (1989) also indicate that in the global structure of a prominence (probably an active one) extended volumes with sizes of the order of the active region or even larger are present with relatively low temperature ($T_\mathrm{e} < 10^4\,\mathrm{K}$) and electron density intermediate between those in the prominence and corona. It is possible that such a volume corresponds to the coronal cavity around the prominence.

3.1.2. Events of 2000/09/04 and 2001/01/14

Like the event of 1997/09/27, discussed just above, the eruptive filament and prominence in the events of 2000/09/04 and 2001/01/14 looked at 5.7 GHz broader than at 17 GHz again. Due to the inhomogeneity and variability of the brightness temperatures of the eruptive filaments at the two frequencies, we cannot conclude unambiguously whether the eruptive filaments underwent cooling or not. We can state, however, that the bulk of an eruptive filament is, at least, not heated.

3.2. Stages of a Prominence/Filament Eruption

Three stages of filament eruptions, known from non-radio observations (see, e.g., the review by Démoulin, Vial 1992), can be distinctly recognized in height-time plots of the presented events. Microwave data together with non-radio ones permit us to look throughout all of these stages and to find some observable features corresponding to them.

1st *stage, a pre-eruptive activation.* A filament ascends very slowly with a constant velocity or with a small acceleration.

This stage was observed in all three events discussed (figures 5a, 8b, and 12b). In the event of 04/09/2000, the eruptive filament was attached to the solar surface with several black strips, which lengthened in the ascension of the filament. They are detectable at 5.7 GHz in the first frame (05:24 UT) of figure 6 and represent filament barbs visible in microwaves. Their direction is the same as the direction of the filament barbs observed in Hα. No conspicuous helical structure was observed in either EUV or microwaves at this stage or before it.

2nd *stage, rapid eruptive acceleration.* The expanding filament takes helical structure. Primary bright kernels appear in the microwave emission. Flare ribbons are not yet present.

In the event of 2000/09/04 observed at 5.7 GHz throughout the whole set of images, the filament-barb structure mentioned was distinctly transformed into the main body of the eruptive filament during this second stage. This transformation was accompanied by the appearance of a rear edge of the eruptive filament, and its helical structure was visible in EUV emission, and can be also detected in 5.7 GHz movies. The appearance of the rear edge of the filament (after about 05:30 UT at 5.7 GHz; see also figure 6) means that the filament barbs detached from the solar surface, and the formation of the eruptive filament itself was completed. The microwave flux started to increase (figure 8a) at about 05:25 UT near the bend of the initial filament in two compact kernels visible also in EUV emission. Only after 05:40 UT, the classical flare ribbons expanded out of these kernels. The microwave flux started to increase at approximately the same time as the filament started to accelerate (dashed line in figure 8b).

3rd *stage, free self-similar expansion.* The filament moves with a high speed, but a small acceleration. Flare ribbons develop.

At this stage, the shapes of the frontal structure and the eruptive filament are similar at different times (figures 7 and 11), and height-time plots of different parts of CME are represented by diverging straight lines (figures 8b and 12b). The acceleration monotonically decreases approaching zero.

Other important features of the discussed events are as follows:

- Both the frontal structure and the core of the 2000 September 4 CME had a twin-loop configuration (figure 7), which probably had a relation to the segmental structure of the initial filament. A similar configuration was observed in the event of 1997 September 27 (figures 1e and 2a). The configuration of the 2001 January 14 CME appeared as a simple single-loop configuration in microwaves. However, this is probably the most massive segment of the CME (similar to the event of 2000/09/04), and its overall structure did not certainly contain a single expanding loop only. This follows from the shape of the accelerated filament observed in EUV and very long EUV flare ribbons observed.
- The bulk of the eruptive prominence was not heated. Its massive body remained cool in all three event discussed. Hot EUV features were observed against the cold body of the microwave eruptive prominence (features “BF3” and “BF4” in figure 6, and a thin shroud visible in EUV emission in figure 9, which coincided with the prominence observed in microwaves).

3.3. Initiation of an Eruption

The qualitative scheme to describe these stages, including the observed participating features, is shown in figure 13, which outlines some points of a Dual-Filament CME initiation model (Uralov et al. 2002; figure 13 is a slightly modified figure 9 from that paper). This model was developed to fit observational data of the filament eruption on 2000/09/04.

The initial filament consists of two or more segments, dextral in this case (the interior of segments observable in Hα is hatched). Two segments tend to merge together to form a single long magnetic structure. The “backbone” coronal magnetic field B_ℓ connects these segments. The upward expansion of this magnetic system is prevented

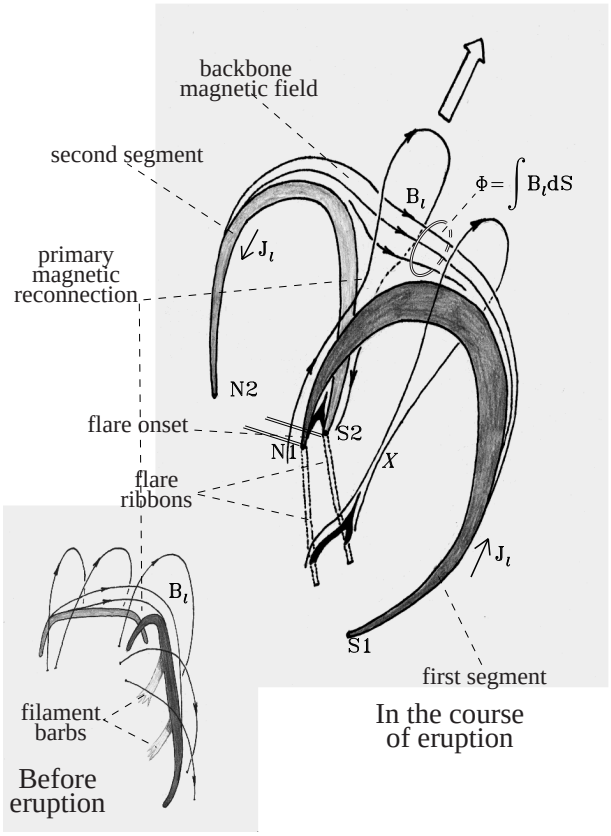

Fig. 13. Dual-Filament CME initiation model. The initial filament consists of two segments connected with a coronal backbone magnetic field B_ℓ. Three factors lead to an MHD instability: (1) primary magnetic reconnection low in the corona just above the cross-point of the segments; (2) barbs tear off from the solar surface to form additional internal helical twist and eruptive filament itself (flux rope); (3) if the lifting force of the 1st and 2nd driving factors is sufficient to extend substantially the overlying coronal arcades, then magnetic reconnection starts under the filament (label X) according to the classical scheme.

by (a) filament barbs attaching the filament to the photosphere (only two barbs are shown in the figure) and (b) overlying coronal arcades. It is worth mentioning that a tendency of two filament segments to merge is realistic. A rapid change in the magnetic connectivity of two different segments of a filament system and the formation of a long filament before its eruption was observed by Kim et al. (2001; see also the scenario in figure 4 from their paper). Three driving factors can lead to a magnetohydrodynamic instability, which would cause the eruption.

First driving factor Due to slow primary magnetic reconnection of the filament segments (or, more precisely, the magnetic envelopes of these segments), the magnetic moment of the "backbone" magnetic field increases. The 1st driving factor comes into existence, and the initial upward motion starts. The situation looks similar to the Tether Cutting model (e.g., Moore et al. 2001), but they differ substantially. In our model, primary magnetic reconnection occurs low in the corona, just above the cross-point of the filament segments visible in Hα, corresponding to the place, where the solar flare will start. Due to this factor, the filament can only rise up to a certain height if the preventing factors, (a) and (b), are conserved. It seems worth mentioning in this connection the paper by Ji et al. (2003), where the authors argue in favor of reconnection above a filament and its failed eruption.

Second driving factor Due to lengthening and magnetic reconnection, filament barbs tear off from the solar surface (not shown in the cartoon) to form a flux rope (internal helical structure with right twist) and the eruptive filament, itself. This creates an additional force directed upwards (similar to the Flux Rope model, e.g., Forbes, Isenberg 1991; Amari et al. 2000). The preventing factor (a) transforms into an expansion supporter, a 2nd driving factor. And, again, the filament can only rise up to some height if the preventing factor (b) is conserved. It is possible that a short-term EUV brightening of the skin of the filament during its acceleration is due to magnetic reconnection of the filament barbs underneath the filament prior to the two-ribbon flare. Probably, this narrow skin plasma remains hot during subsequent expansion of the prominence, which is observed in EUV as a thin bright envelope of the cold prominence core.

Third driving factor If the lifting forces of the first and second driving factors are sufficient to extend overlying coronal arcades substantially, then magnetic reconnection of coronal loops starts under the filament (label X) in accordance with the classical scheme: the external helical structure with a (left) twist appears and grows, and the lifting force increases. Preventing factor (b) transforms into an expansion supporter, the 3rd driving factor. The two-ribbon flare starts.

The magnetic configuration shown in figure 13 looks like a low-lying *quadrupolar* one inside a *large-scale bipolar* magnetic configuration. Primary magnetic reconnection between the segments of the pre-eruptive filament occurs in an X-point of this internal quadrupolar system. Therefore, to initiate primary reconnection, strong, permanent shear motions of filament footpoints are not necessary. Small evolutionary changes in the vicinity of the cross point of the filament segments (observed, e.g., as photospheric magnetic flux cancellation) are probably sufficient. Note in this respect that large shear motions of the photospheric footpoints is the first crucial factor in the Breakout model of a CME initiation (Antiochos et al. 1999). In this model, a low current-carrying *bipolar* arcade is located under an X-separator of a *large-scale quadrupolar* configuration. The magnetic breakout is at work only when the rate of magnetic reconnection at the quadrupole null point is slow, i.e., slower than the rate, at which the system is being sheared. Only under this condition can the sheared magnetic energy be stored. However, magnetic reconnection at the null point is the second crucial factor in the Breakout model. It is introduced to remove unsheared magnetic fields above the low-lying, sheared magnetic flux near the neutral line. On the other hand, the strongly sheared magnetic flux can release its magnetic energy and produce an eruptive flux rope, even without the mentioned condition in the frame-

work of the Flux Rope model (e.g., Amari et al. 2000). Nevertheless, a combination of our empirical dual-filament initiation model with the breakout model seems fruitful. To combine them, one should place our cartoon at the base of a large-scale quadrupole magnetic configuration.

Our model connects the appearance of an additional helicity in the structure of the eruptive filament/prominence with the reconnection and detachment of the filament barbs. Thus, the appearance of a helical structure suggests the onset of the eruption process. It is difficult to predict when the helicity starts to be observable, but it must definitely be the case when the ejecta acquires rapid acceleration.

The change in the expansion velocity observed for the prominence on 1997 September 27 implies some change in the regime of its preparation to the eruption. Although it is difficult to connect this velocity increase with some particular process from the data we have, this phenomenon may be potentially interesting in the context of the initiation of an eruption.

3.4. Expansion of an Ejecta

Using the similarity of shapes and height-time plots of different parts of a CME, one can use an extrapolation of the size and geometry of a CME to estimate its initial parameters. Uralov et al. (2005) proposed a method for that, which is based on comparative measurements of the spatial locations of the eruptive filament and CME frontal structure with a self-similar solution of MHD equations. In particular, this method can be applied to observations of the events of 2000/09/04 and 2001/01/14.

A comparison of the experimental height-time plots with self-similar invariant kinematic plots is demonstrated in figures 8c,d. Uralov et al. (2005) showed that the magnetic structure corresponding to the frontal structure of CME in the event of 2000/09/04 (features "BF1" and "BF2" in figure 6) was relatively low, about 100–150 Mm above the filament before the eruption. The surface extent that participated in the formation of the CME was found to be comparable with the maximal extent of the flare ribbons visible in EUV. The initial (maximum) acceleration was estimated of order a few $\mathrm{km\,s^{-2}}$, greater than the solar gravity acceleration.

In contrast to the on-disk event of 2000/09/04, the estimated initial spatial scale in the off-limb event of 2001/01/14 was > 1000 Mm, and the acceleration of the eruptive prominence was 4–5 times less than the solar gravity acceleration. The acceleration stage continued in this event for more than one hour. These circumstances may have a relation to the possible large, or even increasing, mass of the cool material of the CME mentioned in subsection 2.3. Note that mass loading with new cold material was observed in the event of 1997/09/27 several hours before the eruption (see subsections 2.1 and 3.5).

The self-similar solution (e.g., Low 1982) applies to rather late expansion only, and it cannot correctly describe the initial stages of the eruption. The simplest kinematic relation to describe the velocity U in a self-similar expansion is $U = U_\infty \sqrt{1 - R_0/R}$ with U_∞ being the final velocity, R the distance from the virtual expansion center, and R_0 the initial radius of the ejecta. One can obtain from this relation that the initial acceleration is maximal, and it monotonically decreases during the course of expansion approaching zero (see, e.g., Uralov et al. 2005). On the other hand, the initial acceleration has been known to gradually increase from zero up to its maximum value (e.g., Gallagher et al. 2003). We observed just such a behavior of the acceleration in the event of 2001 January 14, when it initially increased from 10 to $60\,\mathrm{m\,s^{-2}}$, and then, at late stages observed with LASCO, it decreased up to zero, in accord with the self-similar expansion.

3.5. Mass Loading or Emptying?

In the observation on 1997 September 27, the prominence had a distinct dual-loop (two-segment) shape at 22:26 UT (Hα image in figure 2). The appearance of the second loop was possible in two ways, i.e., due to new cool mass loading into the second segment of the ascending prominence, or due to significant cooling of hot plasmas. However, the latter possibility does not seem to be realistic, because the prominence did not show any features in any coronal EUV line (we did not show those images).

The increase of the area of the eruptive prominence observed on 2001 January 14, which is also shown by the growth of its total flux time profile in figure 12c means that either the mass of the cool material of the prominence increased, or it was dense enough to keep its large opacity during the observed expansion.

Thus, our observations rule out a probable emptying the filament before eruption in these events (cf. Low, Zhang 2002), and mass loading seems to be more preferable possibility.

3.6. On the Relation of CMEs and Flares

Currently, CMEs are often classified as CMEs related to flares and CMEs related to filament eruptions. By contrast, Švestka (2001) proposed that the only difference between CMEs is the location of the eruption site: if it is inside an active region, where magnetic fields are strong, then a post-eruptive Hα flare is observed; if beyond active regions, then the magnetic fields are weak, which would result in no pronounced flare.

The event of 2000 September 4 shows an example of an eruption off any active regions, but a subflare was observed there in Hα, microwaves, and soft X-rays. However, it was very weak, and its importance in soft X-rays was C1.5 only. The eruptive event of 2001 January 14 was accompanied by a soft X-ray enhancement of C1.4, but no Hα subflare was registered. Thus, in particular, such eruptions can be followed by very weak subflares, in accord with another statement of Švestka concerning the continuous spectrum of the CME properties.

4. Summary and Concluding Remarks

We have presented and analyzed three microwave observations of pre-eruptive and eruptive prominences and filaments on 1997/09/27, 2000/09/04, and 2001/01/14 with

Nobeyama and SSRT radioheliographs along with Hα, extreme-ultraviolet, and white-light coronagraphic data. The events show three stages of the eruption process: (1) pre-eruptive activation, (2) rapid acceleration, and (3) free expansion of an ejecta. The results are as follows:

1. Taking advantage of multi-spectral observations, particularly at two or three microwave frequencies, we estimated the temperature and density of eruptive prominences and their surroundings;
   - The kinetic temperature of the observed eruptive prominences remains low, ~ 5000 K. All eruptive filaments/prominences observed in the three events did not experience heating in the course of eruption. The brightenings of eruptive prominences observed with SOHO/EIT are probably only due to heating of their thin envelopes.
   - The electron number density in the main body of the prominence before the eruption is about $(1\text{–}3)\cdot 10^{10}$ cm^{-3}.
   - The prominences are surrounded by a cool environment of low density, $n_e \sim (2\text{–}8)\cdot 10^9$ cm^{-3}, probably, cool ($T < 10^4$ K) threads.
   - The thickness of the major layer of the prominence-to-corona transition region, which contributes to microwave emissions, is estimated to be very small, with a characteristic scale of order 5 km.
2. Simultaneous microwave SSRT observations and white-light LASCO observations with overlapping fields of view allowed us to identify the cool radio prominence and a CME core. Thus, we confirmed that a CME core consists of remnants of an eruptive prominence and can remain cool.
3. The emptying of filaments/prominences before an eruption is unlikely. Mass loading into the prominence is more probable.
4. Kinematic characteristics of eruptive prominences confirm an initial increase of acceleration from zero up to its maximum value, and then, at late stages observed with LASCO, it decreases up to zero, in accord with the free self-similar expansion.
5. Extrapolation of a self-similar solution to the solar surface gives a possibility to estimate the initial parameters of a CME. The initial surface extent of a CME was found to be comparable with the maximal extent of the flare ribbons visible in EUV. The initial position of the frontal structure in the September 4, 2000 eruptive event was found to be about 100–150 Mm above the pre-eruptive filament.

We have addressed all stages of the eruption and briefly discussed the observations in terms of our *Dual-Filament CME Initiation Model*, which consists with the observational facts.

We thank H. Nakajima, A. Vourlidas, H. Hudson, and I. Chertok for useful discussions. A. Uralov and V. Grechnev wish to thank the colleagues from NRO and its staff for their help and hospitality during their stays at the Observatory. We appreciate the valuable help of the unknown referee to improve the paper. We are grateful to the instrumental teams of the NoRH, SSRT, Paris and Mauna Loa Observatories, and SOHO mission for their open-data policies. SOHO is a project of international cooperation between ESA and NASA. We also used the CME catalog generated and maintained by NASA and the Catholic University of America in cooperation with the Naval Research Laboratory. This work is supported by the Russian Foundation of Basic Research under Grants 06-02-16239, 06-02-16263, 06-02-16295, 06-02-91161, the Russian Federal Ministry of Education and Science under Grants NSh 477.2003.2 and OFN 18, the Presidium of RAS, the Russian Direction of Federal Scientific and Technical Programs under Grant 112/001/045, and the program of the Russian Academy of Sciences "The solar activity and physical processes in the Sun-Earth system".

References

Amari, T., Luciani, J. F., Mikic, Z., & Linker, J. 2000, ApJ, 529, L49
Antiochos, S. K., DeVore, C. R., & Klimchuk, J. A. 1999, ApJ, 510, 485
Chertok, I. M., & Grechnev, V. V. 2005, Sol. Phys., 229, 95
Chiuderi-Drago, F. 1990, in Proc. IAU Colloq. 117, ed. E. Tandberg-Hanssen (Berlin and New York: Springer-Verlag), 70
Démoulin, P., & Vial, J. C. 1992, Sol. Phys., 141, 289
Dere, K. P., et al. 1997, Sol. Phys., 175, 601
Forbes, T. G., & Isenberg, P. A. 1991, ApJ, 373, 294
Gallagher, P. T., Lawrence, G. R., & Dennis, B. R. 2003, ApJ, 588, L53
Gary, D. E. 1986, in NASA, Goddard Space Flight Center, Coronal and Prominence Plasmas 121-125 (SEE N87-20871 13-92)
Gopalswamy, N., et al. 1998, Geophys. Res. Lett., 25(14), 2485
Gopalswamy, N., & Hanaoka, Y. 1998, ApJ, 498, L179
Gopalswamy, N., Hanaoka, Y., & Lemen, J. R. 1998, in Proc. IAU Colloq. 167, ASP Conf. Ser. 150, 358
Gopalswamy, N. 1999, in Proc. of the Nobeyama Symp., ed. T. S. Bastian, N. Gopalswamy, & K. Shibasaki, NRO Report 479, 141
Gopalswamy, N., Shimojo, M., Lu, W., Yashiro, S., Shibasaki, K., & Howard, R. A. 2003, ApJ, 586, 562
Grechnev, V. V., et al. 2003, Sol. Phys., 216, 239
Hanaoka, Y., et al. 1994, PASJ, 46, 205
Hanaoka, Y., & Shinkawa, T. 1999, ApJ, 510, 466
Hori, K., & Culhane, J. L. 2002, A&A, 382, 666
Illing, R. M. E., & Hundhausen, A. J. 1985, J. Geophys. Res., 90, 275
Ji, H., Wang, H., Schmahl, E. J., Moon, Y.-J., & Jiang, Y. 2003, ApJ, 595, L135
Kardapolova, N. N., Lesovoi, S. V., Borisevich, T. P., Peterova, N. G., & Ryabov, B. I. 2004, in Proc. IAU Symp. 223, 2004, ed. A. V. Stepanov, E. E. Benevolenskaya, & A. G. Kosovichev (Cambridge: Cambridge University Press), 265
Kim, J.-H., Yun, H. S., Lee, S., Chae, J., Goode, P. R., & Wang, H. 2001, ApJ, 547, L85

Kundu, M. R., White, S. M., Garaimov, V. I., Manoharan, P. K., Subramanian, P., Ananthakrishnan, S., & Janardhan, P. 2004, ApJ, 607, 530
Kurochka, L. N., & Kiryukhina, A. I. 1989, Hvar Obs. Bull., 13, 51
Low, B. C. 1982, ApJ, 254, 796
Low, B. C., & Zhang, M. 2002, ApJ, 564, L53
Ma, S. L., Jiang, Y. C., Li, Q. Y., Zhao, S. Q., Li, L. P., & Chen, H. D. 2005, Proc. IAU Symp. 226, ed. K. P. Dere, J. Wang, & Y. Yan (Cambridge: Cambridge University Press), 121
Marqué, Ch., Lantos, P., & Delaboudinière, J.-P. 2002, A&A, 387, 317
Mein, N., Schmieder, B., DeLuca, E. E., Heinzel, P., Mein, P., Malherbe, J. M., & Staiger, J. 2001, ApJ, 556, 438
Moore, R. L., Sterling, A. C., Hudson, H. S., & Lemen, J. R. 2001, ApJ, 552, 833
Nakajima, H., et al. 1994, Proc. IEEE, 82, 705
Ramesh, R. 2005, in Proc. IAU Symp. 226, ed. K. P. Dere, J. Wang, & Y. Yan (Cambridge: Cambridge University Press), 83
Rao, A. P, & Kundu, M. R. 1977, Sol. Phys., 55, 161
Smolkov, G. Ya., Pistolkors, A. A., Treskov, T. A., Krissinel, B. B., & Putilov, V. A. 1986, Ap&SS, 119, 1
Švestka, Z. 2001, Space Sci. Rev., 95, 135
Uralov, A. M., Grechnev, V. V., & Hudson, H. S. 2005, J. Geophys. Res., 110, A05104
Uralov, A. M., Lesovoi, S. V., Zandanov, V. G., & Grechnev, V. V. 2002, Sol. Phys., 208, 69
Zandanov, V. G., & Lesovoi, S. V. 1999, in Proc. Nobeyama Symp., ed. T. S. Bastian, N. Gopalswamy, & K. Shibasaki, NRO Report 479, 37
Zandanov, V. G., Lesovoi, S. V., & Uralov, A. M. 1999, in Structure and dynamic of the solar corona, Proc. Intern. Conf. on Solar Physics (in memory of Prof. G.M. Nikolsky), (Troitsk: IZMIRAN), 236 (in Russian)